A High-Resolution MEMS Piezoelectric Strain Sensor for Structural Vibration Detection

Stanley Kon, *Member, IEEE*, and Roberto Horowitz, *Member, IEEE*

***Abstract*—This paper presents the modeling, fabrication, and testing of a high-performance dynamic strain sensor. Using microelectromechanical systems (MEMS) technology, ZnO piezoelectric microsensors are directly fabricated on silicon and steel substrates. The sensors are intended to be used as point sensors for vibration sensing without putting an extra burden on the host structures. A model that incorporates piezoelectric effects into an RC circuit, representing the sensor architecture, is developed to describe the voltage output characteristics of the piezoelectric microsensors. It is shown that the sensitivity of microplanar piezoelectric sensors that utilize the e_{31} effect is linearly proportional to sensor thickness but unrelated to sensor area. Sensor characterization was performed on a cantilever beam cut from a fabricated silicon wafer. The experimental data indicate that the overall sensor and circuit system is capable of resolving better than 40.3 nanostrain time domain signal at frequencies above 2 kHz. The corresponding noise floor is lower than 200 femto-strain per root hertz and the sensitivity, defined as the sensor voltage output over strain input, is calculated to be 340 V/ε. Micro ZnO piezoelectric sensors fabricated on steel hard disk drive suspensions also show excellent results. The sensor not only has a better signal-to-noise ratio but also detects more vibration information than the combination of two laser-doppler-vibrometer measurements in different directions.**

***Index Terms*—Microelectromechanical systems (MEMS), nanostrain, piezoelectric, strain gauge, strain sensor, vibration, zinc oxide (ZnO).**

I. Introduction

VIBRATION is a common problem for control of mechanical structures as it may generate noise, reduce stability, or decrease positioning accuracy. Many innovations have been made in vibration suppression control to compensate for the unwanted vibrations [1]–[3]. For vibration control to be possible, information from a real time vibration signal is usually needed. At the macro scale, several kinds of sensors have been developed in order to measure strain or corresponding physical properties. Fiber optical sensors measure the change in wavelength or phase of light, and the corresponding strain is calculated accordingly [4], [5]. Although most fiber optical sensors can achieve resolution anywhere from microstrain to nanostrain per root hertz, a major drawback is the bulky optics for conditioning and controlling the light beam. Another common method for strain sensing involves the use of piezoresistive materials, of which the strain change is proportional to the resistance change. Piezoresistive strain gauges are usually applied to structures for static to low frequency strain detection.

From a strain sensing perspective, it is desirable to make sensors much smaller than the host structure. A smaller sensor reduces the burden of the added sensors on the structure, preserving structural dynamics. Smaller sensors can also be used to explore local strain on structures without averaging the strain at the neighborhood. The concept of local strain is especially important in vibration detection as the sensor location [6], [7] determines the kind of vibration information being retrieved [8], [9]. Similar to the node concept on structures, in that nodes show no displacement at a certain resonance frequency, there are also locations on structures that show no strain at certain resonance frequency while exhibiting large strain at other frequencies. The sensor location, if properly chosen, can serve as a weighting function for the sensing signal in frequency domain.

Over the years, microelectromechanical systems (MEMS) techniques have proven to be an efficient way of miniaturizing transducers by orders of magnitude. Various sensors based on strain detection such as pressure sensors [10]–[12], accelerometers [13], [14], or atomic force microscopy sensors [15]–[17] have been developed using MEMS technology. These sensors are typically fabricated on silicon or quartz substrates and installed into a housing for implementation. In addition to their compactness, another advantage of MEMS sensors over macro sensors is that they can be fabricated in batch, minimizing the manufacturing cost.

Most microstrain sensors rely on piezoresistive effects [18] to measure the corresponding strain. Others use capacitance change [19] or frequency shift of a resonator fundamental mode [20] to extract the strain information. Piezoelectric materials [21] such as lead zirconate titanate (PZT), zinc oxide (ZnO), or aluminum nitride (AlN) are seldom used for standalone strain sensors [22], [23] in microscale, although they have been used extensively for MEMS surface acoustic wave (SAW) devices [24], which are composed of both actuators and sensors. Piezoelectric sensors produce charges when subjected to external strain or stress. The signal strength is proportional to sensor thickness. Since MEMS sensors are considerably thinner than bulk devices, MEMS piezoelectric sensors lose sensitivity as a result of their size in comparison with larger devices. MEMS strain sensors are mostly made of piezoresistive materials, which are less vulnerable to size effect, in part because of this

Manuscript received January 28, 2006; revised March 15, 2007; accepted March 16, 2007. Current version published November 19, 2008. This work was supported in part by the National Science Foundation, in part by the Information Storage Industry Consortium, and in part by the Computer Mechanics Laboratory, University of California, Berkeley. The associate editor coordinating the review of this paper and approving it for publication was Prof. Paul Regtien.

The authors are with the Department of Mechanical Engineering, University of California, Berkeley, CA 94720 USA (e-mail: scskon@gmail.com; horowitz@me.berkeley.edu).

Digital Object Identifier 10.1109/JSEN.2008.2006708

reason. However, piezoelectric sensors typically show better signal-to-noise ratio (SNR) over a large frequency range and are more suitable than piezoresistive sensors for vibration signal detection. Piezoelectric sensors are also capable of detecting strains in all directions simultaneously whereas piezoresistive strain gauges are usually used for strain sensing in single direction.

In this paper, the authors explore the ultimate resolution of ZnO MEMS piezoelectric strain sensors for dynamic strain sensing and demonstrate the use of these strain sensors, which are fabricated on both silicon and steel substrates. The paper is organized as follows. In Section II, a dynamic model is constructed to model planar piezoelectric strain microsensors. The model shows the influence of thermal noise and parasitic capacitance on sensing signals. They are found to be the fundamental limitations of sensor resolution. In Section III, the fabrication of ZnO piezoelectric sensor on silicon substrates is detailed. The fabrication process is then tailored to fabricate sensors on steel substrates; these substrates are transformed into more complex hard disk drive suspensions. Experimental setups and results are described in Section IV. It is shown that, when the sensing signal is properly handled, piezoelectric sensors are superior to the laser-dopper-vibrometer (LDV) in dynamic signal sensing.

II. Theory

A. Piezoelectricity

The electrical–mechanical cross coupling of piezoelectric materials is usually described by two constitutive equations. When used as sensors, piezoelectric materials transform mechanical energy into electrical signals. This phenomenon, called the direct piezoelectric effect, can be expressed using one of the constitutive equations as

$$D_i = e_{ij}S_j + \varepsilon_0\varepsilon_{ik}^{S}E_k \tag{1}$$

where D, e, S, ε, and E are electrical displacement, strain piezoelectric coefficient, mechanical strain, material permittivity, and electric field, respectively. The constant $\varepsilon_0 = 8.854 \times 10^{-12}$ F/m is the permittivity of the free space. The subscripts $i = 1, 2, 3$, $k = 1, 2, 3$, and $j = 1, 2, 3, 4, 5, 6$ denote the direction to which physical properties are related. For instance, e_{ij} is the piezoelectric coefficient that describes the charge collected in the plane perpendicular to i direction due to the applied strain in the j direction. The superscript in ε_{ik}^{S} denotes the permittivity at constant strain. The piezoelectric coefficient matrix e_{ij} is a three-by-six matrix in general, but, for materials such as ZnO or PZT, the matrix can be written into a special form

$$e = \begin{pmatrix} 0 & 0 & 0 & 0 & e_{15} & 0 \\ 0 & 0 & 0 & e_{15} & 0 & 0 \\ e_{31} & e_{31} & e_{33} & 0 & 0 & 0 \end{pmatrix}. \tag{2}$$

The three-direction is taken as the polar axis. Since microfabricated sensors are usually two-dimensional structures, it is assumed the polar axis is in the out-of-plane direction and only D_3 can be measured. The electrical displacement, D_3, is the charge

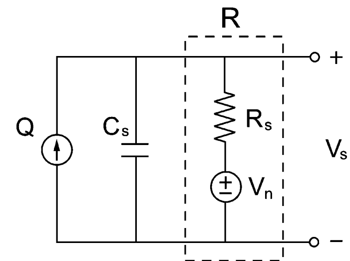

Fig. 1. Equivalent circuit model for a piezoelectric microsensor.

collected on both electrodes of the piezoelectric material and effectively forms a capacitor, which can also be written as

$$D_3 = \frac{Q}{A} \tag{3}$$

where Q and A are charge and sensor area, respectively. Without external electric fields, the above equations can be simplified as

$$D_3 = e_{31}(S_1 + S_2) + e_{33}S_3. \tag{4}$$

Hence, the total charges measured per unit area is the sum of normal strain in all directions multiplied by different piezoelectric constants.

B. Sensor Modeling

Several assumptions were made to simplify the modeling. First, it is assumed that the sensor is subjected to exactly the same strain as that on the structure surface. This is reasonable because the sensor is much thinner than the substrates with negligible interfacing layers between the sensor and the structure. Secondly, sensor transient response [26] resulting from acoustic waves inside the sensor is neglected. The frequencies of these propagation and reflection waves in the sensor are much higher than structural vibration frequencies of interest. The waves are considered insignificant and not included in the modelling. Furthermore, it is assumed that the sensors are small enough that no modal sensing [27] comes to effect. In other words, the sensor is treated as a point sensor and strain is uniformly distributed over the area covered by the sensors.

As shown in Fig. 1, a piezoelectric sensor can be modeled as a charge source Q in parallel with a capacitor C. A resistor R in parallel is also included in the model to represent the leakage current path for sensor-generated charges. The resistor is decomposed into an ideal resistor R_s and a noise voltage source V_n. Using Kirchoff's law, the sensor output V_s in the frequency domain is calculated as

$$V_s = \frac{\mathrm{IR}_s}{sR_sC + 1} = \frac{sR_s}{sR_sC + 1}Q \tag{5}$$

where $s = jw$ is the Laplace variable and $I = (\mathrm{d}Q/\mathrm{d}t)$ is the current generated by the strain sensor as a result of external loads. The current can be written as $I = sQ$ in the Laplace domain. With the additional assumption that only in-plane strain S_1 and S_2 are applied to the sensor, (3)–(5) can be combined into

$$V_s = \frac{sR_sAe_{31}}{sR_sC + 1}(S_1 + S_2). \tag{6}$$

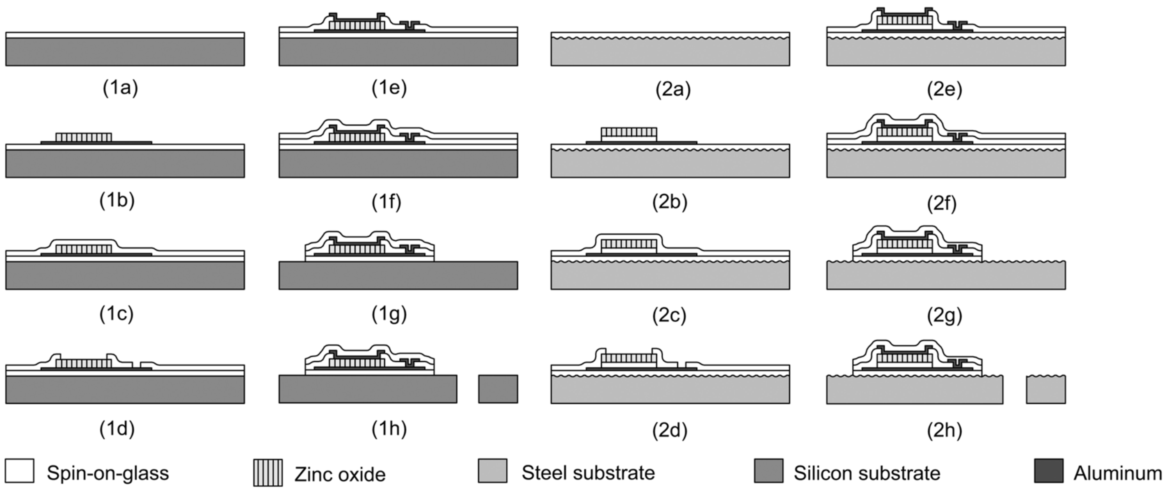

Fig. 2. Process flow of sensor fabrication on silicon (1a)–(1h) and steel substrates (2a)–(2h).

TABLE I
COMPARISON OF ZnO AND COMMON MICROFABRICATION COMPATIBLE PIEZOELECTRIC MATERIALS [25], [24] WITH $t = 1\ \mu$m

	e_{31} (C/m^2)	c_{11} (GPa)	ε_{33}^S	$\frac{e_{31}t}{\varepsilon_0\varepsilon_{33}^S}$ (kV)
PZT-5H	-6.5	12.6	1470	-0.50
ZnO	-0.57	20.97	10.2	-6.31
AlN	-1.02	36	10.4	-11.07

The noise at the sensor output can be calculated similarly

$$V_{sn} = \frac{1}{sR_sC+1}V_n \tag{7}$$

where V_n is the noise source with spectral density

$$v_n = \sqrt{4k_BTR_s} \tag{8}$$

and k_B is Boltzmann's constant.

Several observations are made from the above equations. Equation (6) shows that piezoelectric strain sensors act like high-pass filters for strain input. The high-pass nature of the sensors makes them less responsive to low frequency strain inputs. At low frequencies, the generated charges tend to leak through the sensor before being amplified by the circuit. Equation (7) shows that thermal noise enters the system as if into a low-pass filter. Both equations indicate that piezoelectric sensors are superior in detecting dynamic signal at higher frequencies.

Neglecting the noise term and plugging in the sensor capacitance relation $C = A(\varepsilon_0\varepsilon_{33}^S/t)$, (6) can be expressed as follows at high frequencies:

$$V_s = \frac{Ae_{31}}{C}(S_1+S_2) = \frac{e_{31}t}{\varepsilon_0\varepsilon_{33}^S}(S_1+S_2) \tag{9}$$

where t is the sensor thickness. The equation shows that the voltage output of an ideal piezoelectric sensor requires high piezoelectric coefficient with low permittivity. A thicker sensor geometry would also provide better sensitivity. Table I compares physical properties of several common piezoelectric materials. Note that although PZT is usually considered the best piezoelectric material for actuation due to its high piezoelectric coefficients, the high permittivity makes it less attractive a material for strain sensing applications than ZnO or AlN. For a given mechanical input, ZnO and AlN essentially trade current/charge for higher voltage output than PZT. In this paper, ZnO is chosen over AlN as the piezoelectric sensing material for its better fabrication compatibility.

At lower frequencies, (6) can be written as

$$V_s = sR_sAe_{31}(S_1+S_2) = s\rho e_{31}t(S_1+S_2) \tag{10}$$

where ρ is the ZnO film resistivity. The voltage output becomes a function of resistivity rather than permittivity. For ZnO, as the inverse of its material permittivity is much larger than the resistivity, the sensor will usually be much less responsive at lower frequencies. In addition, the sensor output is linearly proportional to the signal frequency. In the limiting case where a static strain is applied on the sensor, the sensor would show zero output voltage to external strain input.

III. FABRICATION OF ZnO PIEZOELECTRIC SENSOR

A. Sensor Fabrication on Silicon Substrates

The piezoelectric sensor fabrication process is begun by spin coating a 0.7-μm-thick spin-on-glass (SOG) on the silicon substrate, as shown in Fig. 2(1a). The substrate is baked at 260 °C for 15 minutes to cross link the SOG layer. The SOG insulation layer is optional for building sensors on silicon wafers but is crucial for that on steel substrates, which will be explained in the next section.

After SOG coating, an aluminum layer is evaporated to form ohmic contacts [28] and patterned, followed by ZnO sputtering; see Fig. 2(1b). The ZnO layer is deposited using RF magnetron sputtering at 300 °C with 200 W forward power in 35-mtorr oxygen and 35-mtorr argon. The deposition rate is around 0.8 μm per hour. It is found that ZnO films of approximately 0.8 to 1 μm are good enough for sensing purpose. The ZnO film is patterned using a mixture of phosphoric acid, acetic acid, and a water solution with 1:10:100 ratio in volume. Then, a second SOG layer is spin coated and patterned; see Fig. 2(1c)–2(1d).

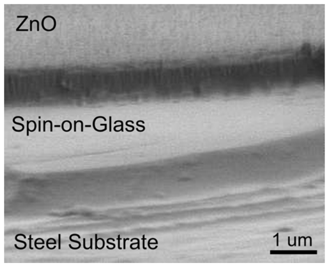

Fig. 3. Scanning electron microscopy (SEM) picture of a ZnO film deposited on a SOG planarized steel substrate.

The top electrode is evaporated and patterned; see Fig. 2(1e). The last SOG is spin coated to encapsulate the sensor and patterned; see Fig. 2(1f)–2(1g). Finally, the wafer is cut into strips using bulk micromachining or by dicing; see Fig. 2(1h).

B. Sensor Fabrication on Steel Substrates

Fabricating sensors on steel substrates is a much more difficult process. The suspension design to which the steel substrates will be transformed requires that the steel wafers are limited to 38-μm thickness and as a result is highly susceptible to deformation during fabrication processes. For instance, vacuum chucks have been found to cause permanent deformation in steel wafers over the course of normal wafer processes. This deformation, in turn, causes film thickness to vary across the substrate and propagates these error ensuing processes. To solve this problem, steel wafers are water bonded to silicon handle wafers. Adhesion can be adjusted by controlling the amount of water trapped between the two wafers. When the process is finished, the two wafers are heated to 100 °C to evaporate the water between wafers and release the steel substrate.

Another problem is associated with the thermal expansion coefficient of steel, which is an order of magnitude larger than most microfabrication compatible materials. The mismatch results in large residual stresses, causing adhesion problems after thin-film deposition. Hence, the temperature throughout the fabrication process needs to be carefully controlled and kept as low as possible. One of the major reasons for selecting ZnO over AlN as the strain sensor material is that piezoelectric ZnO films can be deposited at temperatures as low as 300 °C, whereas AlN requires deposition temperature at least 100 °C higher.

Steel oxidization during high temperature processing also causes problems. Oxidation occurs during ZnO deposition because of the elevated temperature and the presence of oxygen in the chamber. Steel substrates are already very rough from a microfabrication viewpoint, as is visible in Fig. 3. Oxidation causes the surface to become even rougher, which makes it impossible to deposit ZnO films with good piezoelectric properties. A smooth surface [29] is crucial to piezoelectric ZnO film growth. To obtain a planar surface, SOG is spin coated onto the steel substrate and baked. The SOG layer not only planarizes the steel substrate but also prevents the substrate from oxidation on the front side. At present, the oxidation on the back side is ignored, where no microscale processing takes place.

After an SOG layer is coated onto the steel substrate [Fig. 2(2a)] an aluminum layer is evaporated and patterned for bottom electrode [Fig. 2(2b)]. Then, a second SOG layer is coated. The advantage of using this additional SOG layer is two fold. First, the SOG layer serves as the buffer layer for the ZnO and aluminum layer, reducing residual stress gradient. It is found that the ZnO layer does not adhere to aluminum well under high thermal residual stress. The presence of the SOG layer provides a smoother stress gradient between ZnO and aluminum. Secondly, the SOG planarizes the aluminum layer for better ZnO deposition. The SOG is able to smooth out the surface again after aluminum deposition and provide a much better condition for ZnO deposition.

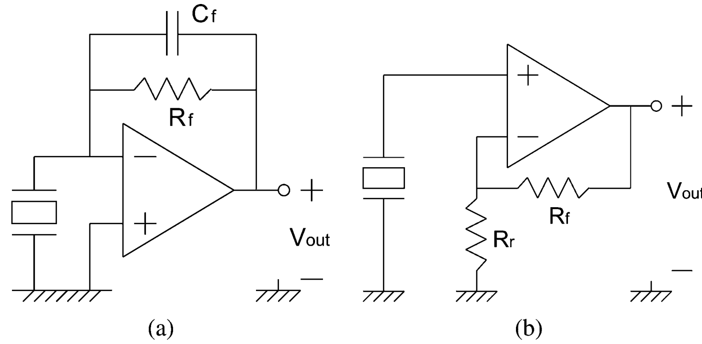

Fig. 4. Conventional (a) inverting (transimpedance) and (b) noninverting amplifier.

Using the same deposition and etching recipe as those used in Section III-A, a 0.8-μm ZnO layer is deposited on top of the second SOG layer and patterned. The SOG layer sandwiched between the ZnO and bottom electrode layer is dry-etched in SF_6 plasma [Fig. 2(2b)]. This is a self-aligned process as the ZnO layer is used as the mask. The rest of the process, Fig. 2(2c)–2(2g), is the same as that used in the previous section. After sensor fabrication, the steel wafer is etched through using bulk micromachining, Fig. 2(2h) and assembled into hard drive suspensions for testing [30].

IV. EXPERIMENTAL SETUP AND RESULTS

A. Interface Circuit

As shown in the modeling section, a piezoelectric sensor is essentially a capacitor in parallel with a charge source and a large resistor. The presence of the capacitance makes sensor output impedance much larger than that of data acquisition systems operating at lower frequencies, which effectively reduces sensor sensitivity. To minimize this problem, an interface circuit is needed to convert high sensor impedance into low impedance. The circuit also amplifies the sensing signals and rejects unwanted noises.

Fig. 4(a) and (b) shows two commonly used single stage circuit topologies for amplification of piezoelectric sensing signals. Since our devices are intended to detect less than 100 nanostrain with a corresponding current of approximately pico-to-subpico ampere, neither of the circuits is capable of amplifying the sensing signals. The transimpedance amplifier, shown in Fig. 4(a), relies on resistor R_f to convert sensor current to voltage $V_{\text{out}} = I \cdot R_f$. Capacitor C_f is used to stabilize the circuit as transimpedance amplifiers are prone to oscillating if not properly compensated. In our case, the feedback resistor

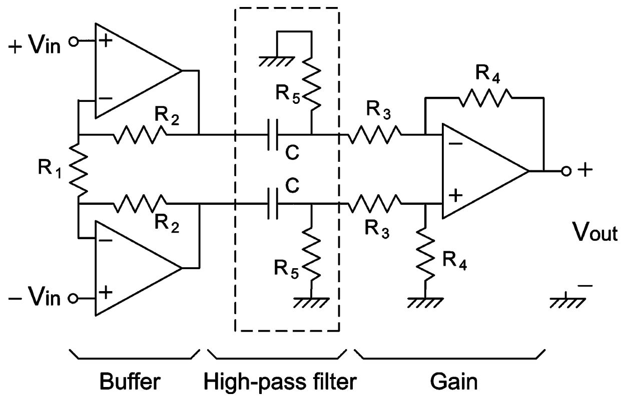

Fig. 5. The interface circuit for sensor signal amplification is composed of a differential input stage, a high-pass filter, and a gain stage. Resistors R_5 are redundant which are used to adjust the high-pass corner frequency predetermined by R_3, R_4, and C. Component values: $R_1 = R_5 = 100\ \Omega$, $R_2 = 5\ k\Omega$, $R_3 = 1\ k\Omega$, $R_4 = 10\ k\Omega$, and $C = 1.5\ \mu$F.

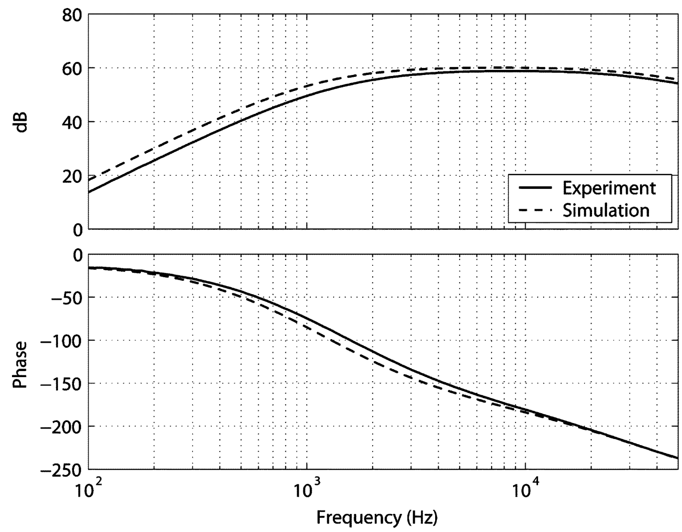

Fig. 6. Transfer function of the interface circuit used for sensor signal amplification.

R_f needs to be extremely large for reasonable voltage output. This is not practical both because large R_f reduces bandwidth and the compensating C_f needs to be unpractically small. The amplifier with a large R_f also considerably amplifies the environmental noise coming from the noninverting end which saturates the circuit.

Another way to utilize this configuration is to use only C_f in the feedback loop. This is commonly called a charge amplifier where the voltage gain is set by the ratio of input capacitance and the feedback capacitor $A = (C_s/C_f)$. While charge amplifiers work well for macropiezoelectric sensors, they are not suitable for our experimental setup as the amplification is achieved by using a feedback capacitor smaller than the input capacitance. To amplify a sensing signal on the fabricated ZnO sensors, this requires a feedback capacitor of 10 pF (for unity gain) or less, which is difficult to implement in practice. Such small a capacitor is very vulnerable to parasitic capacitance. *A priori* knowledge of the tested sensor capacitance is also needed so that a proper feedback capacitor can be implemented accordingly. This makes the charge amplifier undesirable for testing the prototyped ZnO sensors, as the sensors vary in different sizes and ZnO film properties vary from sensor to sensor.

Noninverting amplifiers, shown in Fig. 4(b), use resistors R_f and R_r to set the amplification gain $A = 1 + (R_f)/(R_r)$. This amplifier has a much larger input impedance than that of a inverting amplifier which makes it a better choice for amplifying device signals with small current. The amplifier is used to form the differential input stage of the interface circuit shown in Fig. 5. The interface circuit is composed of three stages with an overall circuit gain of 1000. With this large gain, efforts are made to prevent the circuit from saturation due to unwanted noise. A differential input stage is utilized for better common mode signal rejection. Common mode signals at the input are found to be one of major signal sources that saturate the circuit. A high-pass filter at the second stage is used to heavily penalize low frequency signals, such as the dc offset from the operational amplifiers or 60-Hz environmental noise. This stage cuts off signals below a certain frequency and ensures that signals passed through the last gain stage do not saturate the circuit. Since only vibrations above 100 Hz are of interest, it would be ideal to filter out all signals below this frequency. In reality, the circuit gradually filters out signals below 2 kHz. As low frequency vibration modes are usually associated with larger amplitudes, inducing larger strain and sensor signals, the slope between 100 Hz to 2 kHz provides a robust way to prevent circuit saturation in practice. The double-to-single end converter at the last stage of the circuit serves as the gain stage. The root-mean-square (rms) and peak-to-peak noise of the circuit are found to be 6.3 and 43.2 mV, respectively. Fig. 6 shows the simulated and experimental circuit transfer functions. The discrepancy between the simulation and the measurement at low frequencies is attributed to component, especially capacitor, mismatch due to tolerance, which causes the corner frequency to shift from the designed frequency.

Since these sensors are intended for nano-to-micro strain sensing, very limited charges are generated by piezoelectric sensors. The sensing signal is both very vulnerable to environmental noise and susceptible to attenuation through its signal path. Parasitic capacitance is found to be the main factor that can drastically lower sensitivity. The parasitic capacitance C_p can be modeled as an additional shunt capacitor in parallel with C_s in Fig. 1. Using (5), the voltage into the circuit is

$$V_s = \frac{sR_s}{sR_s(C_s + C_p) + 1} Q. \tag{11}$$

For decent signal retrieval, C_p needs to be smaller than the sensor capacitance. As C_p becomes larger than C_s, the signal starts to decrease at a rate inversely proportional to C_p. Therefore, the key for successful measurement is to put the circuit sufficiently close to the sensor. All connections need to be made so that parasitic capacitance is minimized. Coaxial cable, for instance, introduces approximately 25 pF/ft capacitance and should not be used to connect the sensor and the circuit. It is found that properly buffering and amplifying the sensing signal before passing it to the acquisition system dramatically increases sensor sensitivity and system robustness.

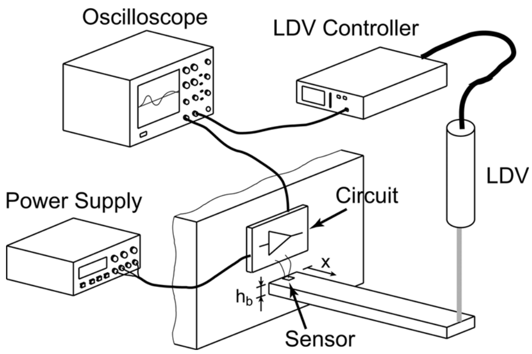

Fig. 7. The experimental setup used for strain sensor characterization.

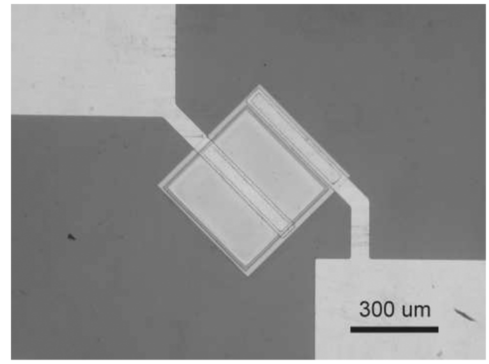

Fig. 8. A 380 × 380-μm piezoelectric ZnO strain sensor fabricated on a silicon substrate.

TABLE II
SUMMARY OF SENSOR PARAMETERS AND EXPERIMENTAL RESULTS

Beam	Length	L_b		4.2 cm
	Width	w_b		3.3 mm
	Height	h_b		0.5 mm
	Young's modulus	E_b		150 GPa
	Density	ρ		2330 Kg/m^3
	Resonance modes		Calculation	Experiment
		1st	368	420 Hz
		2nd	2300	2140 Hz
Sensor	ZnO thickness	t_s		0.8 μm
	Overall thickness	t_a		4.2 μm
	Length	L_s		380 μm
	Width	w_s		380 μm
	Sensitivity			340 V/ε
	Piezo. coefficient	e_{31}		-3.77$\times 10^{-2}$C/m^2
	Noise Floor		0.3 $\sim$ 50 kHz	200$\sim$70 f$\varepsilon/\sqrt{Hz}$
			Frequency	Resolution
	Measured		2140 Hz	40.3 nε
	Estimated		10,000 Hz	28.7 nε

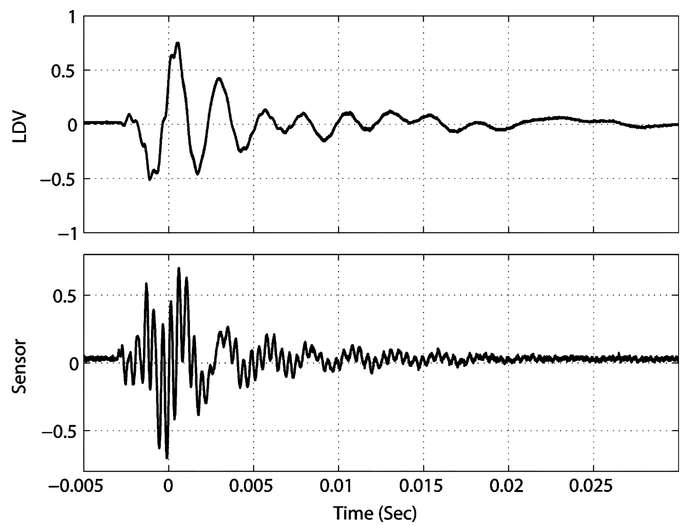

Fig. 9. LDV and sensor measurements of the cantilever when an impulse is applied at the baseplate.

B. Sensors Fabricated on Silicon Cantilever Beams

1) Sensor Signal Verification: A strip cut from the silicon wafer with completed sensors is installed as a cantilever beam on a housing, shown in Fig. 7. The cantilever is installed in such a way that the piezoelectric strain sensor is located at the cantilever support where the most cantilever vibration information can be collected. The sensor and beam dimensions are listed in Table II. The sensor being tested, shown in Fig. 8, is a 380 by 380-μm-square sensor with 4.2-μm overall thickness, including the ZnO film, electrode layers, and passivation layers. The vibration signal is passed to the nearby circuitry through bonded wires. The wires are 31 μm in diameter, having a negligible effect the cantilever vibration modes. A laser-Doppler-vibrometer (LDV) is used to verify the sensor signals. The LDV measures the vertical displacement at the tip of the cantilever. Both LDV signals and amplified sensor signals are connected to an oscilloscope for recording.

The first experiment is performed to verify whether or not the sensor detects the vibration signal that is measured by the LDV. A mechanical impulse is applied on the housing which simultaneously excites several vibration modes of the cantilever beam, shown in Fig. 9. The responses from the sensor and the LDV measurements are very similar to each other, except that higher order modes appear to be more prominent in the sensor measurement. This is due to the higher gain of the interface circuit at high frequencies. Both curves clearly show the first two resonance modes at 419.76 Hz and 2.14 kHz, respectively. The third mode at 6.09 kHz is barely distinguishable. The theoretical values for the corresponding modes are calculated using the following equation [31]:

$$w = (\beta_n L)^2 \sqrt{\frac{E h_b^2}{12 \rho L^4}} \tag{12}$$

where w, L, E, h_b, ρ, and n are resonance frequency in radian per second, beam length, Young's modulus, beam height, beam density, and mode number. The value of β is related to boundary conditions and mode numbers. For single cantilevers, the products $\beta_n L$ are 1.875, 4.694, and 7.855 for the first three resonance modes, respectively. The theoretical value for the first three resonance modes are calculated as 368, 2300, and 6450 Hz. Hence, the amplifier sensor signals are indeed the vibration information from the cantilever.

2) Piezoelectric Constant Characterization: The piezoelectric constant e_{31} is calculated by comparing the amplitude of time domain signals of the LDV and sensor measurements. As mentioned in Section II-B, piezoelectric sensors show different voltage responses at high and low frequencies. It is desirable to characterize piezoelectric response at higher frequencies since the sensors are more responsive at that range. This calculation is also easier because the dynamic model can be approximated to an algebraic equation; see (9).

For the above reasons, the second resonance mode signal is chosen for piezoelectric constant calculation. The lower resonance mode is filtered out by a high-pass filter and the amplitude of the filtered signals are recorded. Sensor signal V_s is evaluated by dividing the amplified sensor signal by circuit gain. LDV signal amplitude is also converted to cantilever displacement y, and the strain at the cantilever base is evaluated using classical beam theory. Assuming small displacement, strain and cantilever tip displace can be related as follows:

$$S(x) = \bar{y}\frac{\mathrm{d}^2 y}{\mathrm{d}x^2} = \frac{h_b}{2}\frac{\mathrm{d}^2 y}{\mathrm{d}x^2} \quad (13)$$

where $\bar{y}$ and x are the distance from neutral line and the distance from the support in the length direction. The displacement under free vibration [31] is

$$y(x) = Cn[\sin(\beta_n x) - \sinh(\beta_n x) - \alpha_n(\cos(\beta_n x) - \cosh(\beta_n x))] \quad (14)$$

where C_n is a normalized constant and

$$\alpha_n = \frac{\sin(\beta_n L) + \sinh(\beta_n L)}{\cos(\beta_n L) + \cosh(\beta_n L)}. \quad (15)$$

Combining (9) and (13), e_{31} can be expressed as

$$e_{31} = \frac{2\varepsilon_0 \varepsilon_{33}^S V_s}{y''(x_s) h_b t_s} = \frac{2\varepsilon_0 \varepsilon_{33}^S}{y''(x_s) h_b t_s}\frac{V_o}{G} \quad (16)$$

where $y''(x_s)$ denotes the double derivative of (14) evaluated at sensor location x_s with constants taken from (15). V_o, G, and V_s are the amplified sensor signal at interface circuit output, circuit gain, and sensor signal, respectively.

The piezoelectric constant e_{31} is found to be 0.0377 C/m^2, which is about an order of magnitude smaller than that reported by most literatures [25], [32]. This small piezoelectric constant may be attributed to two causes. First, the aluminum layer that the ZnO film deposited on is not ideal for ZnO growth. Due to processing equipment problems, the aluminum layer appears a dull and gray color, suggesting a relatively rough surface. Secondly, the parasitic capacitance in the experimental setup also reduces the piezoelectric constant, as explained in Section IV-A. The corresponding sensitivity from strain to sensor voltage output, which is easily evaluated from (9), is found to be 340 V/ε.

3) System Resolution: Fig. 10 shows another set of data collected using the method similar to that described in the previous section. Both the LDV signal and the amplified sensor noise are also plotted for comparison. The resolution of the sensor is clearly superior to that of the LDV, as it can resolve as little as 0.017 V at the sensor-circuit system output, where the LDV barely shows any response. The 0.017 V peak-to-peak signal at 2.14 kHz corresponds to a 26.8-μV sensor output or 80.6 nε. In other words, the sensor is able to resolve at least $80.6/2 = 40.3$ nε vibration signal. Based on the circuit transfer function, the number is further improved to 28.7 nε if the vibration signal were measured at 10 kHz, where the circuit gain is at its maximum. However, to make a beam with this high-resonance frequency is impractical as the resonance of cantilever is inversely proportional to the square of its length, (12). This would require a corresponding beam length of 2 mm in length, for which vibration is very hard to observe.

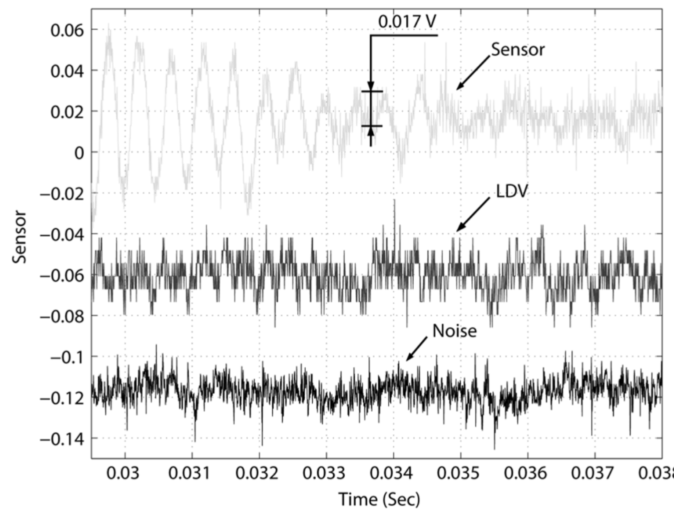

Fig. 10. The best peak-to-peak resolution resolved by the sensor. Both the LDV and amplified sensor noise are also plotted but downshifted from their dc. The noise signal is not captured concurrently with the sensor and LDV signal.

Sensor resolution can also be expressed with respect to the noise floor. The overall noise floor of the system varies between 6 and 30 nV/$\sqrt{\mathrm{Hz}}$, which translates to a sensor resolution of 200 fε/$\sqrt{\mathrm{Hz}}$ at 300 Hz and gradually improves to 70 fε/$\sqrt{\mathrm{Hz}}$ at 50 kHz. The variation in noise floor, hence sensor resolution, results from the nonconstant interface circuit gain and the different noise contribution from resistors and operational amplifiers. Since the circuit gain is much larger at higher frequencies, the noise floor corresponds to a better resolution in this range even though the noise floor is also slightly higher. A summary of sensor characteristics and the beam geometries is listed in Table II.

C. Hard Drive Suspension Sensors

To demonstrate the use of the ZnO piezoelectric sensors in real applications, sensors are fabricated on steel substrates using the process flow described in Section III-B and the substrates are transformed into hard disk drive suspensions. The sensor geometry is designed using a simplified LQG optimization algorithm [9], resulting in a sensor area of 95924 μm^2, or 66% of the sensor size in the previous section. The suspension is composed of several steel pieces welded together to meet the performance requirements of the hard drives. The suspension is attached to one end of an E-block and is driven by a voice-coil-motor (VCM) located at the other end of the E-block; see Fig. 11.

A network analyzer is used to measure the transfer function from the VCM to the amplified sensor signal. Two LDV measurements are carried out to verify the sensor signal. The LDV

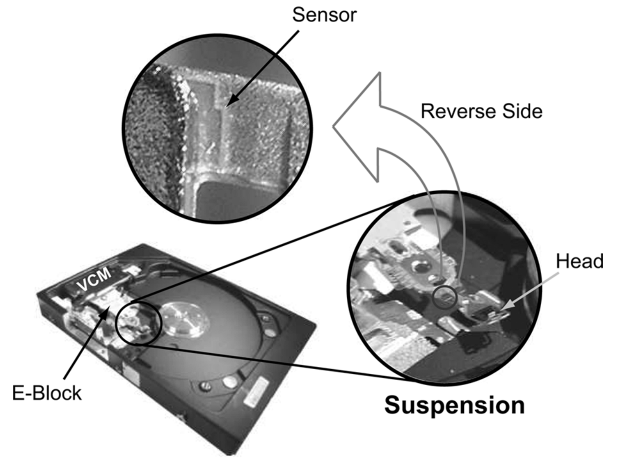

Fig. 11. Fabricated strain sensor on the steel hard drive suspension. Bottom left: A hard disk drive with a VCM, E-block and suspension installed. Right: A close view at the suspension. Top: A closer view at the sensor, which is located on the reverse side of the suspension.

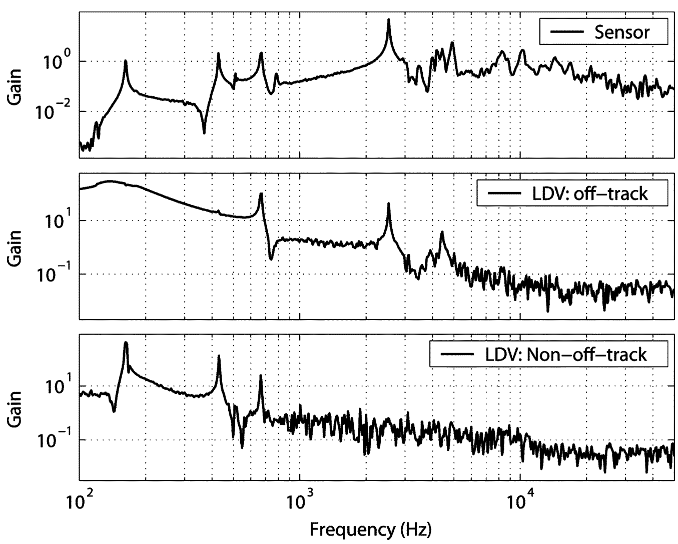

Fig. 12. The suspension transfer function measurements from VCM to sensor, LDV off-track, and LDV nonoff-track.

is first aligned to the suspension tip horizontally to measure its off-track vibration. Then, the LDV is aligned vertically for nonoff-track measurement. The results are shown in Fig. 12. It is found that sensor detects more vibration information than any single LDV measurement. All vibration modes in LDV plots also appear in the sensor plot. The sensor plot shows at least two more vibration modes near 10 kHz that are missing in the LDV measurements. The curve in the sensor plot is also smoother in general, suggesting a better signal-to-noise ratio. This is not surprising as sensors already showed better performance during the cantilever test; see Fig. 10.

V. Conclusion

A model for a microscale piezoelectric strain sensor is developed. It is shown that the model can be reduced to an algebraic equation at higher frequencies where the sensor is more responsive and output voltage is unrelated to sensor size. At lower frequencies, the thermal noise becomes more dominant and sensor output voltage becomes a function of frequency, both of the causes resulting in a lower sensitivity.

ZnO piezoelectric strain sensors are successfully fabricated on both silicon and steel substrates. The fabricated silicon wafers are diced into cantilevers for sensor characterization while the fabricated steel substrates are transformed into hard drive suspensions for testing. An interface circuit is found to be the key to achieving high strain resolution because of the limited charge generated by these microsensors.

The sensitivity of the ZnO piezoelectric sensors is found to be 340 V/ε. Time domain strain signal as small as 40.3 nε at 2 kHz is observed on an oscilloscope. The sensor resolution varies slightly between 2 to 50 kHz with a best resolution of 28.7 nε at 10 kHz. Alternatively, if overall noise floor of the system is defined as the sensor resolution, the resolution would be $30 \sim 200$ f$\varepsilon/\sqrt{\text{Hz}}$, depending on the signal frequency. The hard disk drive suspension manufactured from fabricated steel wafers also shows remarkable response. The measurements show that sensor signals contain more vibration information and have better SNR as compared to LDV results.

Acknowledgment

The authors would like to thank Dr. K. Oldham for valuable discussions and R. Ruzicka from Hutchinson Technology, Inc., for the help in instrumented suspension manufacturing.

References

[1] Y. Li, R. Horowitz, and R. Evans, “Vibration control of a pzt actuated suspension dual-stage servo system using a pzt,” *IEEE Trans. Magn.*, vol. 39, no. 2, pp. 932–7, Mar. 2003.
[2] W. Zhang, G. Meng, and H. Li, “Adaptive vibration control of micro-cantilever beam with piezoelectric actuator in MEMS,” *Int. J. Advanced Manuf. Technol.*, vol. 28, no. 3–4, pp. 321–327, 2006.
[3] H. Tjahyadi, F. He, and K. Sammut, “Multi-mode vibration control of a flexible cantilever beam using adaptive resonant control,” *Smart Materials Structures*, vol. 15, no. 2, pp. 270–278, 2006.
[4] G. Meltz, W. Morey, and W. Glenn, “Formation of Bragg gratings in optical fibers by a transverse holographic method,” *Opt. Lett.*, vol. 14, pp. 823–825, 1989.
[5] B. Lee, “Review of the present status of optical fiber sensors,” *Optical Fiber Technol.*, vol. 9, no. 2, pp. 57–79, Apr. 2003.
[6] K. Hiramoto, H. Doki, and G. Obinata, “Sensor/actuator placement for vibration control using explicit solution of algebraic riccati equation,” *J. Sound Vibration*, vol. 229, no. 5, pp. 1057–1075, 2000.
[7] J. Juang and G. Rodriguez, “Formulations and applications of large structure actuator and sensor placements,” in *Proc. YPI&SU/AIAA Symp. Dynamics Control Large Flexible Spacecraft*, 1979, pp. 247–262.
[8] C. Yatomi, S. Kondoh, and K. Inoue, “The positioning of sensors and actuators in the vibration of flexible systems,” *JSME Int. J.*, vol. 33, pp. 145–152, 1990.
[9] K. Oldham, S. Kon, and R. Horowitz, “Fabrication and optimal strain sensor placement in an instrumented disk drive suspension for vibration suppression,” in *Proc. Amer. Control Conf.*, 2004, pp. 1855–1861.
[10] E. R. Peake, A. R. Zias, and J. V. Egan, “Solid-state digital pressure transducer,” *IEEE Trans. Electron Devices*, vol. ED-16, no. 10, pp. 870–876, Oct. 1969.
[11] S. Sugiyama, T. Suzuki, K. Kawahata, K. Shimaoka, M. Takigawa, and I. Igarashi, “Micro-diaphragm pressure sensor,” in *Technical Dig. Int. Electron Devices Meeting*, 1986, pp. 184–187.
[12] W. P. Eaton and J. H. Smith, “Micromachined pressure sensors: Review and recent developments,” *Smart Materials Structures*, vol. 6, no. 5, pp. 530–539, Oct. 1997.
[13] L. M. Roylance and J. B. Angell, “Batch-fabricated silicon accelerometer,” *IEEE Trans. Electron Devices*, vol. 26, no. 12, pp. 1911–1917, 1979.

[14] P. W. Barth, F. Pourahmadi, R. Mayer, J. Poydock, and K. Petersen, "A monolithic silicon accelerometer with integral air damping and over-range protection," in *Techical Dig. Solid State Sensor and Actuator Workshop*, 1988, pp. 35–38.
[15] A. J. Brook, S. J. Bending, J. Pinto, A. Oral, D. Ritchie, H. Beere, M. Henini, and A. Springthorpe, "Integrated piezoresistive sensors for atomic force-guided scanning hall probe microscopy," *Appl. Phys. Lett.*, vol. 82, no. 20, p. 3538, 2003.
[16] M. Tortonese, R. C. Barrett, and C. F. Quate, "Atomic resolution with an atomic force microscope using piezoresistive detection," *Appl. Phys. Lett.*, vol. 62, no. 8, p. 834, 1993.
[17] F. J. Giessibl and B. M. Trafas, "Piezoresistive cantilevers utilized for scanning tunneling and scanning force microscope in ultrahigh vacuum," *Rev. Scientific Instruments*, vol. 65, no. 6, p. 1923, 1994.
[18] I. Igarashi, "Semiconductor dynamic sensors," *Sensors Actuators*, vol. 13, no. 1, pp. 53–62, Jan. 1988.
[19] M. Suster, J. Guo, N. Chaimanonart, W. H. Ko, and D. J. Young, "Low-noise CMOS integrated sensing electronics for capacitive MEMS strain sensors," *Proc. IEEE 2004 Custom Integrated Circuits Conf.*, pp. 693–696, 2004.
[20] K. Wojciechowski, B. Boser, and A. Pisano, "A MEMS resonant strain sensor operated in air," in *Proc. 17th IEEE Int. Conf. Micro Electro Mechanical Systems*, 2004, pp. 841–845.
[21] G. T. Kovacs*, Micromachined Transducers Sourcebook*. New York: McGraw-Hill, 1998.
[22] P. L. Chen, R. S. Muller, and A. P. Andrews, "Integrated silicon PI-FET accelerometer with proof mass," *Sensors Actuators*, vol. 5, no. 2, pp. 119–126, Feb. 1984.
[23] P.-L. Chen, R. S. Muller, R. D. Jolly, G. L. Halac, R. M. White, A. P. Andrews, T. C. Lim, and M. E. Motamedi, "Integrated silicon microbeam PI-FET accelerometer," *IEEE Trans. Electron Devices*, vol. ED-29, no. 1, pp. 27–33, Jan. 1982.
[24] *Surface Wave Filters*, H. Matthews, Ed. New York: Wiley, 1977.
[25] *Handbook of Thin Film Materials*, H. S. Nalwa, Ed. Boston, MA: Academic, 2002, vol. 3.
[26] M. Redwood, "Transient performance of a piezoelectric transducer," *J. Acoustical Soc. Amer.*, vol. 33, no. 4, pp. 527–536, Apr. 1961.
[27] C.-K. Lee, W.-W. Chiang, and T. C. O'Sullivan, "Piezoelectric modal sensor/actuator pairs for critical active damping vibration control," *J. Acoust. Soc. Amer.*, vol. 90, no. 1, pp. 374–384, 1991.
[28] T. E. Murphy, J. O. Blaszczak, K. Moazzami, W. E. Bowen, and J. D. Phillips, "Properties of electrical contacts on bulk and epitaxial n-type ZnO," *J. Electronic Mater.*, vol. 34, no. 4, pp. 389–394, Apr. 2005.
[29] J. B. Lee, S. H. Kwak, and H. J. Kim, "Effects of surface roughness of substrates on the c-axis preferred orientation of ZnO films deposited by r.f. magnetron sputtering," *Thin Solid Films*, vol. 423, no. 2, pp. 262–266, 2003.
[30] S. Kon, K. Oldham, R. Ruzicka, and R. Horowitz, "Design and fabrication of a piezoelectric instrumented suspension for hard disk drives," *Proc. Smart Structures Materials 2006: Sensors and Smart Structures Technologies for Civil, Mechanical, Aerospace Systems*, pp. 951–960, 2006.
[31] S. S. Rao*, Mechanical Vibrations*. Englewood Cliffs, NJ: Prentice-Hall, 1993.
[32] G. Carlotti, G. Socino, A. Petri, and E. Verona, "Acoustic investigation of the elastic properties of ZnO films," *Appl. Phys. Lett.*, vol. 51, no. 23, pp. 1889–1891, Dec. 1987.

Stanley Kon (S'05–M'07) received the B.S. degree in mechanical engineering from National Taiwan University, Taipei, Taiwan, in 1999. He is currently working towards the Ph.D. degree in mechanical engineering at the University of California, Berkeley.

His research interests include smart materials, micro-sensors and actuators, semiconductor manufacturing, vibration control, and mechatronics.

Roberto Horowitz (M'89) was born in Caracas, Venezuela, in 1955. He received the B.S. degree (highest honors), in 1978, and the Ph.D. degree in mechanical engineering from the University of California, Berkeley, in 1983.

In 1982, he joined the Department of Mechanical Engineering, University of California, Berkeley, where he is currently a Professor. He teaches and conducts research in the areas of adaptive, learning, nonlinear and optimal control, with applications to microelectromechanical systems, computer disk file systems, robotics, mechatronics, and intelligent vehicle and highway systems.

Dr. Horowitz is a member of ASME.